SANDIA REPORT

SAND2014-19465
Unlimited Release
Printed November 2014

GADRAS Detector Response Function

Dean J. Mitchell, Lee T. Harding, Gregory G. Thoreson, and Steven M. Horne

Prepared by
Sandia National Laboratories
Albuquerque, New Mexico 87185 and Livermore, California 94550

Sandia National Laboratories is a multi-program laboratory managed and operated by Sandia Corporation, a wholly owned subsidiary of Lockheed Martin Corporation, for the U.S. Department of Energy's National Nuclear Security Administration under contract DE-AC04-94AL85000.

Issued by Sandia National Laboratories, operated for the United States Department of Energy by Sandia Corporation.

Available to DOE and DOE contractors from
U.S. Department of Energy
Office of Scientific and Technical Information
P.O. Box 62
Oak Ridge, TN 37831

Telephone: (865) 576-8401
Facsimile: (865) 576-5728
E-Mail: reports@adonis.osti.gov
Online ordering: http://www.osti.gov/bridge

Available to the public from
U.S. Department of Commerce
National Technical Information Service
5285 Port Royal Rd.
Springfield, VA 22161

Telephone: (800) 553-6847
Facsimile: (703) 605-6900
E-Mail: orders@ntis.fedworld.gov
Online order: http://www.ntis.gov/help/ordermethods.asp?loc=7-4-0#online

SAND2014-19465
Unlimited Release
Printed November 2014

GADRAS Detector Response Function

Dean J. Mitchell, Lee T. Harding, Gregory G. Thoreson,
and Steven M. Horne, Nuclear Threat Science, 6634
Sandia National Laboratories
P.O. Box 5800
Albuquerque, New Mexico 87185, MS-0782

Abstract

The Gamma Detector Response and Analysis Software (GADRAS) applies a Detector Response Function (DRF) to compute the output of gamma-ray and neutron detectors when they are exposed to radiation sources. The DRF is fundamental to the ability to perform forward calculations (i.e., computation of the response of a detector to a known source), as well as the ability to analyze spectra to deduce the types and quantities of radioactive material to which the detectors are exposed. This document describes how gamma-ray spectra are computed and the significance of response function parameters that define characteristics of particular detectors.

CONTENTS

FIGURES

NOMENCLATURE

API	Application Programming Interface
CdTe	cadmium telluride
$CdWO_4$	cadmium tungstate
Cs_2LiYCl_6:Ce	CLYC
CZT	cadmium zinc telluride
DRF	Detector Response Function
GADRAS	GAmma Detector Response and Analysis Software
HPGe	High Purity Germanium
keV	kiloelectron-volts
MCNP	Monte Carlo N-Particle
MeV	Megaelectron-volts
NaI	sodium iodide

1. INTRODUCTION

The GAmma Detector Response and Analysis Software (GADRAS) evolved from an application that was originally developed in 1986 to compute the response of sodium iodide (NaI) detectors [1]. The Detector Response Function (DRF) was subsequently generalized to incorporate other scintillators, as well as semiconductor detectors such as High Purity Germanium (HPGe) [2]. The DRF in the current version of GADRAS applies a combination of first-principals calculations and empirical models to enable fast and accurate computation of the spectral response for a broad range of gamma-ray detectors [3]. Many of the response function parameters have exact physical significance. For example, the type of detector material and its dimensions are entered directly. Default parameters that are applied when new detector folders are created provide reasonable estimates for characteristics such as resolution and radiation scattering, and they can be quite good if the characteristics are cloned from other detectors of the same type. Computed spectra vary smoothly when response function parameters are adjusted, which permits the application of nonlinear regression to refine the agreement between computed spectra and calibration measurements acquired with a particular detector. The DRF for a characterized detector includes all of the interactions of the radiation with both the detector and the environment; specification of a radionuclide and its activity is sufficient to reproduce all of the spectral features, including the continuum that is created by gamma-rays that undergo Compton scattering with the floor or walls before striking the detector. Alternatively, the scatter calculations can be suppressed when the DRF processes input files generated by external radiation transport codes that already incorporate scattered radiation.

This paper describes the DRF for gamma-ray detectors and the parameters that define the detector characteristics. The response function for neutron detectors is described elsewhere [4]. This document also describes the Application Programming Interface (API), which enables an external application to access the GADRAS DRF.

2. RESPONSE FUNCTION DESCRIPTION

2.1 Computational Approach

Gamma-rays interact primarily with electrons in a detector, and the recoiling electrons undergo further interactions that induce light emission in scintillators or an electric current in semiconductor detectors. The gamma-ray energies are inferred indirectly by recording events that are associated with the transfer of energy to electrons. Three fundamental types of interactions occur within detectors. The first type of interaction is photoelectric absorption, where the incident photon is completely absorbed and all of the energy is transferred to an energetic photoelectron. The electron is ejected from one of the bound shells of the atom in which the interaction occurred. In addition to the photopeak, X-ray escape peaks may also be observed in some cases [5]. Photoelectric interactions are dominant for low-energy (< ~200 keV) gamma-rays. The second interaction is Compton scattering. In this interaction, the incoming gamma-ray is deflected with respect to its original direction, and a portion of the energy is transferred to a recoil electron. While the cross section for photoelectric absorption decreases rapidly with increasing photon energy, the Compton scattering cross section falls off gradually. Compton scattering becomes the most probable interaction between ~200 keV and ~5 MeV for typical gamma-ray detectors. In the third main interaction, the photon can form an electron-positron pair while interacting with the coulomb field of a nucleus. This interaction occurs when the gamma-ray energy exceeds twice the rest mass energy of an electron (1022 keV). The cross section for this process, called pair production, increases with photon energy and is dominant for energies greater than ~5 MeV in most detectors. The energetic charged particles produced by these interactions generally dissipate their kinetic energy within detector material, but the 511 keV gamma-rays that are emitted by positron annihilation may escape.

The processes described above produce spectral distributions for which the most characteristic features are photopeaks corresponding to complete absorption of all of the secondary particles within the detector. However, most interactions for photons exceeding a few hundred keV deposit only a fraction of their energy within the detector. Multiple interactions often occur, which result in spectral continua from cascades of events that involve some or all of the fundamental interactions. When radiation is measured with small detectors or detectors with only low atomic number constituents, such as plastic scintillators, measured spectra may only exhibit continua with small or no apparent photopeaks.

Probabilities for each of the interactions can be computed by applying published cross sections and elemental compositions of the detector materials [6]. However, exact solutions for the ensemble of interactions are computationally intensive, and physical descriptions seldom contain sufficient detail to model all of the interactions with the desired accuracy. The approach that GADRAS uses to obtain fast and accurate response calculations involves the following:

- Use first-principals calculations where possible,
- Apply approximate solutions when associated errors are small,
- Interpolate pre-computed tables to describe phenomena that are tractable but time-consuming based on first-principals calculations, and
- Apply empirical models to account for residual differences.

2.2 Photopeaks and the Compton Continuum

Computation of the photopeak probability and the Compton continuum derived from incomplete absorption of the photon energy is an example of a calculation that combines all four techniques described in Section 2.1. Calculations proceed as follows. Interactions with photons striking the detector surface are sampled with respect to distance from the axis (r) in the vertical and horizontal directions. The path length through the detector, l, is a function of r and the detector shape. The transmission probability for an un-scattered photon is given by the following product:

$$T = \prod_{i=1}^{n} e^{-\mu_i \omega_i \rho l} \tag{1}$$

where: n is the number of elements in the detector, μ_i is the attenuation coefficient of element i, ω_i is the weight fraction of element i, and ρ is the density of the detector material. The total interaction probability, which is equal to (1-T), is obtained simply by computing the area-weighted sum of the interaction probabilities across the face of the detector. The total interaction probability is a first-principals calculation that requires negligible computation time.

The ratio of the photoelectric cross section to the total cross section yields the probability for obtaining a full-energy peak upon the first-interaction, but the total photopeak probability also includes multiple Compton scattering events followed by full absorption of the scattered photon. Computation of Compton scattering events applies several simplifications. The first simplification is that detectors are modeled as if they have rectangular cross sections transverse to the incident radiation. The symmetry implies that only one quadrant of the detector needs to be modeled. The detector is sampled along the vector associated with the incident photons, but calculations show that the population distribution as a function of depth for higher-order scatter events is approximately the same as the first scatter event, which eliminates the need to re-compute the density distribution in the axial direction. Calculations are performed as a series of nested loops that compute probabilities for photoelectric absorption of the scattered photon, and probability distributions for additional scatter events. The angles through which gamma-rays scatter are correlated with the energies of the incident and scattered photons [7]; so the probability distributions represent the angular distributions of the scattered photons for the first- and second-scatter events. However, the angular distribution is essentially isotropic after gamma-rays have scattered twice within the detector. Therefore, probabilities for escape, absorption and scattering in subsequent interactions can be described by average probabilities that only depend on the photon energies. Consequently, the inner loops execute quickly. GADRAS computes a total of six scatter events explicitly, and then extrapolates to estimate the probabilities for twelve scatter events.

Figure 1 illustrates the influence of multiple scatter events on the computed spectrum for a 2″×2″ PVT detector. Multiple scattering increases the total energy deposited in the detector relative to the Compton edge associated with a single interaction. The shape of the Compton continuum below 500 keV is in reasonably good agreement with the measured spectrum after two interactions, but additional scatter loops are required to reproduce the total continuum with high fidelity. Probabilities for photopeaks versus Compton continua may be influenced significantly by cascades with as many as ten scatter events.

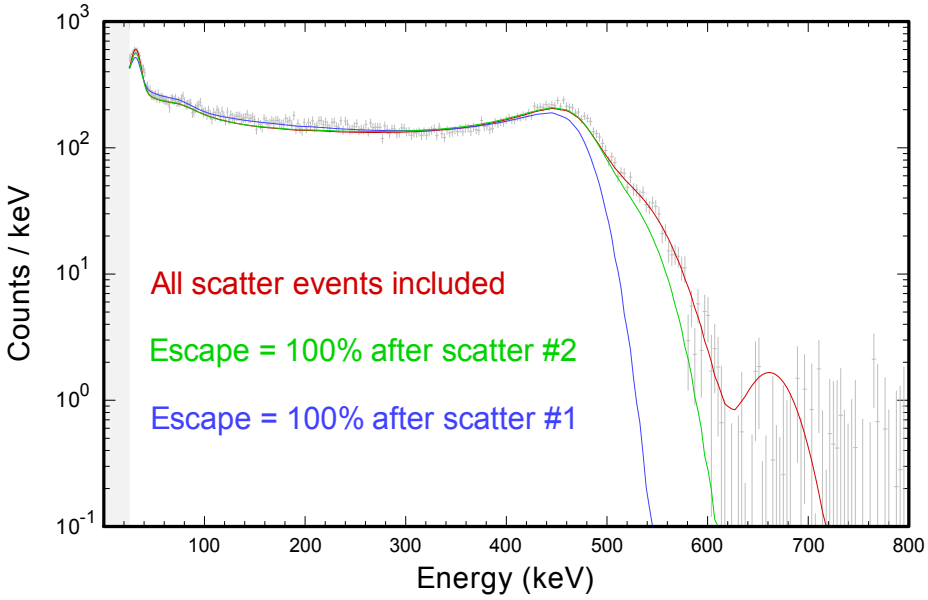

Figure 1. Comparison of computed spectra versus the measured spectrum (gray) for a 2″×2″ PVT detector exposed to a ^{137}Cs source. The blue and green curves represent computed spectra when the escape probability is set to 100% following the first and second scatter events, respectively. The red curve includes all scatter events.

In addition to effects associated with the escape of scattered photons, the energetic electrons produced by photoelectric absorption and Compton scatter events have non-zero probabilities for escape before depositing all of their energies within the detector. The estimated deficit associated with electron leakage is represented in the Compton continuum. This effect is generally small, so rather than assuming the computational burden associated with addressing electron leakage explicitly, an empirical model is used to approximate effects associated with electron leakage. After taking all of these factors into account, observed count rates in the regions between photopeaks and the Compton edge generally exceed the computed continuum in this energy region. Spectra that are computed by Monte Carlo N-Particle (MCNP) or GÉANT also exhibit comparable differences relative to measurements on the low-energy sides of photopeaks. The cause for this discrepancy has not been determined conclusively; so an empirical correction is applied to compensate for these differences.

As discussed in this section, computation of the Compton continuum includes first-principals calculations, approximations where possible, and empirical representations of relatively unimportant effects or phenomena that are not well understood. Even though considerable effort was expended to accelerate calculations, the computation time for a typical spectrum would still be on the order of seconds; whereas the objective is to compute spectra in milliseconds. Additional acceleration is obtained by interpolating a series of continuum calculations (stored in "Response.win" files in detector folders) that are only recomputed when relevant response function parameters change. Accordingly, a typical calculation comprises interpolation of the spectral continuum followed by the addition of photopeaks and escape peaks using tabulated peak intensities.

2.3 Radiation that Scatters into the Detector

Green's functions are used to interpolate MCNP calculations to estimate the profile of scatter radiation as a function of source-detector distance, detector height, and environment clutter [8]. The clutter term varies as the inverse of the distances to walls and other objects. This component of the scattered radiation, called environmental scatter, can be estimated reasonably accurately by applying default scatter values. Figure 2 compares computed spectra for an HPGe detector with measurements at distances ranging from 50 cm to 200 cm. The distance is the only response function parameter that was varied to compute the spectra. The detector and source were both supported on low-mass stands, and the average distance between the detector and the walls was 3 meters when these spectra were measured.

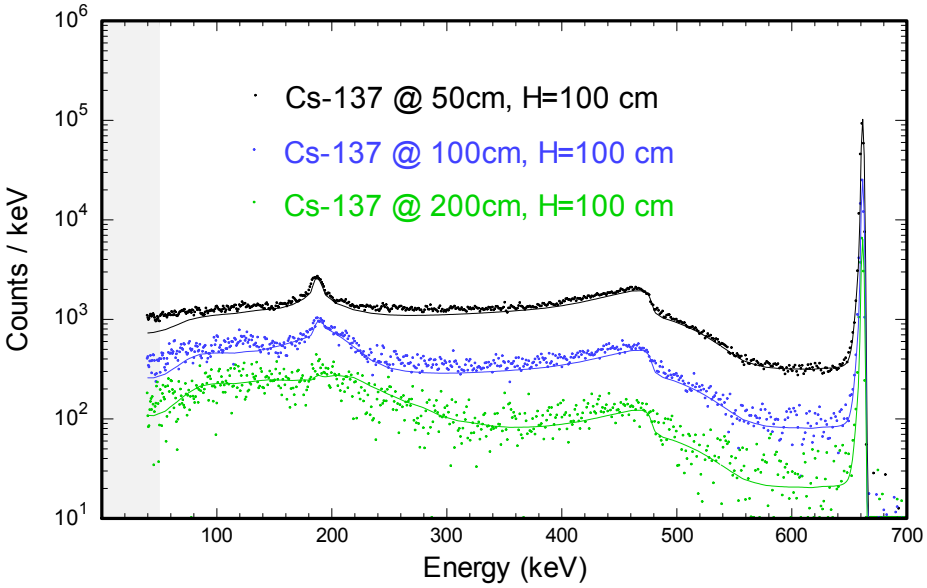

Figure 2. Computed spectra (lines) are compared with measurements (dots) recorded by the HPGe detector at three distances at a height of 100 cm.

The spectra displayed in Figure 2 were recorded under well-controlled conditions, which is not always the case. For example, either the source or the detector is often placed on a table that interacts with some of the radiation. This creates an ambiguity about whether the floor or the surface of the table should be selected as the proper reference point for the height. Detector housings may also contribute local scattering that is not represented by the environmental scatter term. As a result, the computed environmental scatter generally underestimates the total incidence of scattered radiation. Several empirical parameters can be adjusted to improve the accuracy of computed spectra for a specific detector or environmental condition. The empirical model for these effects was developed by observing characteristics for about 100 detectors over a wide range of conditions. The adjustable parameters are generally used to describe additional scattering needed to reproduce observed spectra. First-order effects associated with changes in distance or height are estimated reasonably accurately for the environmental component of the scattered radiation; however, estimates for the local component may not be accurate under conditions that differ from the original characterization measurements.

2.4 Single and Double Escape Peaks

Single and double escape peaks at 511 keV and 1022 keV below the full-energy peaks are prominent features in spectra when high-energy gamma-rays strike detectors. Pair production generally occurs as the first interaction, with the relative probability being the ratio of the pair production cross section to the total cross section. Positrons annihilate within a short distance of their point of origin, so positron annihilations can be assumed to correspond to the first interaction density profile as a function of depth within the detector. The positrons have forward momentum when they are created, but are essentially at rest when they annihilate with electrons within the detector. The two 511 keV gamma-rays travel in opposite directions, but the orientation of the pair of gamma-rays is random with respect to the vector of the original gamma-ray. Therefore, computing escape probabilities is a simple matter of averaging the interaction probabilities throughout the detector volume; the only complication associated with this calculation is that the two gamma-rays travel in opposite directions; if one ray has a short path length to the surface of the detector, the other is likely to have a long path length. Less obvious spectral features resulting from pair production are produced when one or both of the 511 keV gamma-rays undergo Compton scattering before exiting the detector. As illustrated in Figure 3, these scatter events add to the continuum in the region extending from 1022 keV below the photopeak to the full energy of the incident gamma-ray.

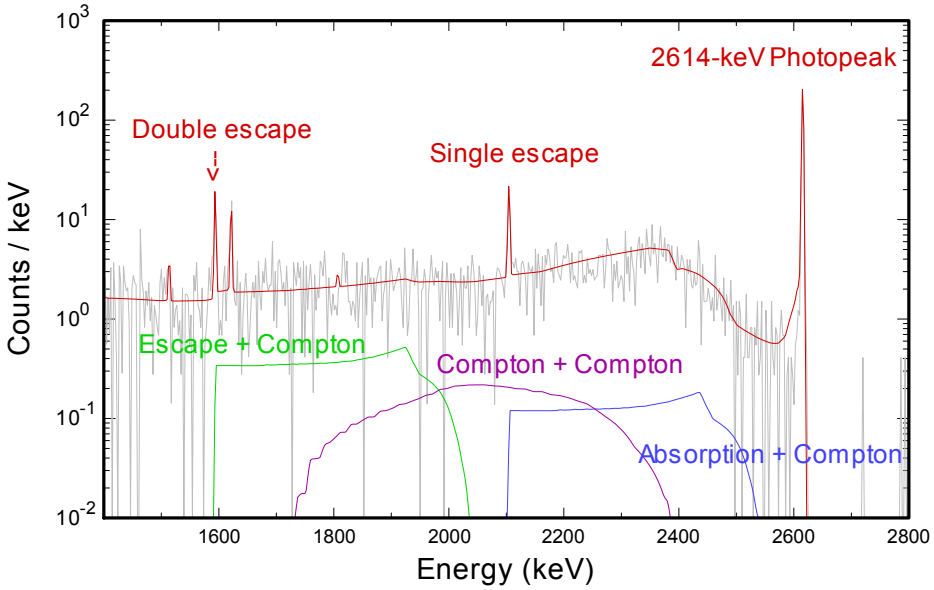

Figure 3. The spectrum recorded by an HPGe detector exposed to a ^{232}U source (gray) is compared with the computed spectrum (red). Components associated with Compton scattering of one or both 511 keV gamma-rays are superimposed.

2.5 Neutron Interactions with Gamma-Ray Detectors

Neutrons produce a response when they interact with gamma-ray detectors, and the characteristics of the response differ for each detector material. Neutron interactions with HPGe detectors are particularly interesting because neutron absorption, which is the dominant reaction for low-energy neutrons, produces a continuum that extends to 10.2 MeV; high-energy neutrons

produce characteristic inelastic scattering features. Therefore, HPGe detectors function as two-channel neutron detectors (this is generally viewed as an annoyance rather than a benefit). Although a small peak at 10.2 MeV may be observable with a sufficiently long count time, the continuum is the dominant feature associated with neutron absorption because the gamma-rays that are shed by the excited nucleus are likely to escape either directly or after Compton scattering. In contrast, inelastic neutron scattering produces a series of saw-tooth features extending from 600 keV to 1600 keV. Figure 4 compares the computed contribution derived from neutron interactions with a measured spectrum that was recorded while a 140% HPGe detector was exposed to a plutonium source within a 0.5-inch thick polyethylene moderator. The fission gamma-ray continuum represents a substantial portion of the total response in this energy region (although this is magnified by the log-scale). Neutron absorption accounts for almost all of the spectral response above about 8 MeV.

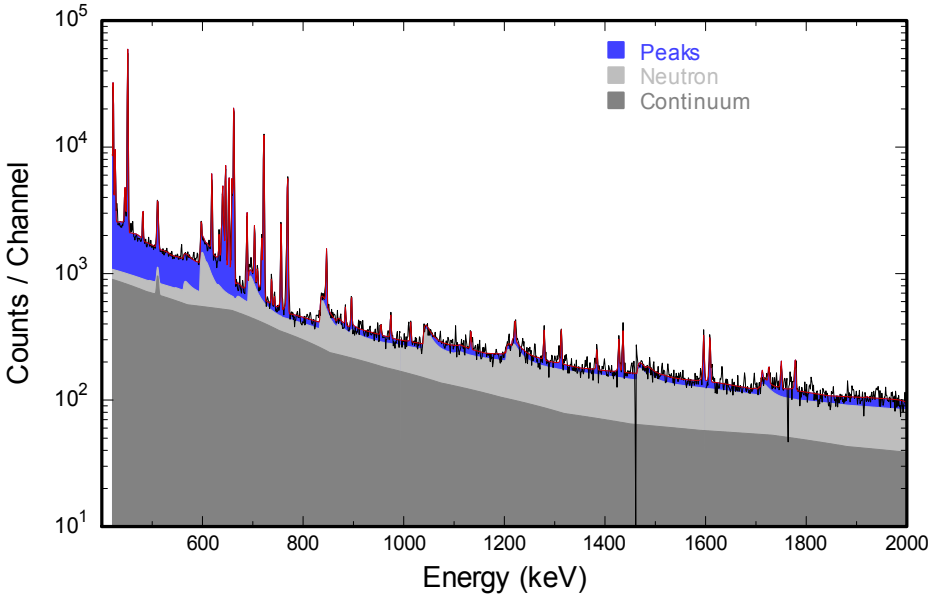

Figure 4. Filled regions in this plot represent components of the spectrum produced when an HPGe detector is exposed to plutonium. The dark gray region is associated primarily with fission gamma-rays. The light gray region represents neutron interactions, which are composed of the saw-tooth features plus a continuum that extends to 10.2 MeV. The measured spectrum is black and the red trace shows the computed spectrum, which is the sum of all of the spectral components.

GADRAS applies a combination of first-principals calculations and empirical adjustments to compute effects associated with neutron interactions. The average neutron interaction probability is calculated using the neutron absorption and/or inelastic scattering probability. These interaction probabilities are calculated using published cross sections and integrating over the neutron energy profile. This provides a reasonable estimate for the dependence of the associated spectral features on neutron energy. However, empirical adjustments are necessary in almost every case to match observed spectral features. For example, the shape of the neutron absorption continuum in HPGe varies with the size of the crystal due to differences in the gamma-ray escape probabilities. Details regarding multiplicity and correlated energy profiles of gamma-rays

that are emitted by the excited germanium nuclei are not known, so first-principals calculations could not be performed with the available data even if computational burden were not deemed to be excessive. Therefore, empirical continuum profiles are interpolated based on the detector volume relative to archived measurements for large and small HPGe detectors. Substantial adjustments were also required to match observed intensities for the 19 inelastic neutron scatter components observed in HPGe.

In addition to continua, neutron exposure produces discrete peaks in spectra recorded by detectors besides HPGe. For example, cadmium emits several gamma-rays upon neutron absorption, which produce photopeaks in CZT, CdTe, and $CdWO_4$ detectors. Peaks can also be produced by the emission of charged particles, as is the case for CLYC (Cs_2LiYCl_6:Ce), which exhibits a peak at a gamma-ray equivalent of 3.3 MeV following the reaction $n+{}^6Li \rightarrow {}^3H+{}^4He$. These emissions are modeled as internal sources that are assumed to originate uniformly throughout the detector material.

Each detector type has unique response characteristics, but computation of these effects is entirely automated. All that is required from the user's perspective is the neutron profile incident on the detector.

2.6 X-Ray Escape Peaks

When photoelectric absorption occurs, an energetic photoelectron is ejected from a bound shell of an atom with an energy that is equal to the difference between the incident gamma-ray energy and the original binding energy of the photoelectron. The most probable origin of the photoelectron is from one of the K shells (the most tightly bound shells) of the atom [7]. An electron from a less tightly bound shell drops into the produced vacancy almost immediately, and an X-ray is emitted. The majority of the X-rays are absorbed within the detector, so this process normally results in deposition of the total gamma-ray within the detector. However, there is a non-zero probability that the X-ray will escape; this is most likely to occur when detectors are exposed to low-energy gamma-rays, which are absorbed near the surface of the detector. GADRAS employs an analytic model to compute the X-ray escape probability [5]. Completion of this calculation takes several seconds, but the calculation is only performed when new detector materials are added. During normal calculations, a table of X-ray escape probabilities is interpolated to obtain yields for the appropriate peaks. X-ray escape is only significant for low-energy gamma-rays, where the photoelectric effect dominates the cross section. Figure 5 shows an HPGe spectrum that exhibits distinct X-ray escape peaks. Although X-ray escape is also computed for other types of detectors, it is often difficult to distinguish X-ray escape features from photopeaks and scatter continua for low-resolution detectors.

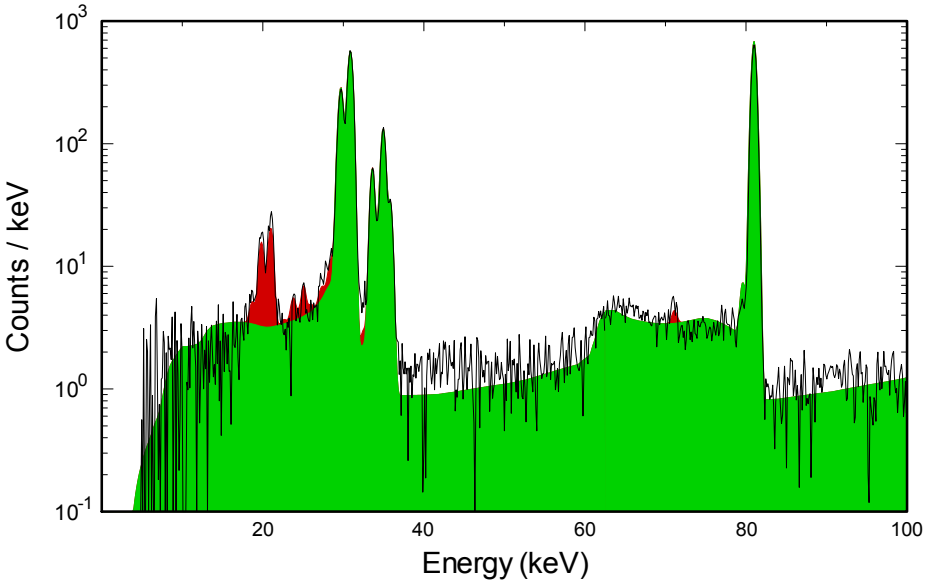

Figure 5. The measured spectrum for a combination of ^{131}Xe, ^{131m}Xe, ^{135}Xe and ^{133m}Xe, which is represented by the black curve, is compared with computed spectra. The green spectrum shows a calculation that neglects X-ray escape peaks. The red regions represent the escape peaks. Intensities of full-energy peaks are reduced slightly as a result of X-ray escape.

2.6 Peak Shapes

Most scintillators exhibit photopeaks that can be described by symmetric Gaussian distribution, which are completely defined by area, mean and resolution parameters. HPGe detectors often exhibit a tail on the low-energy side of a peak, which GADRAS describes by means of "low-E skew" parameters. Detectors such as CZT exhibit skew on both low- and high-energy sides of photopeaks. We have not been able to identify an analytic expression that can represent the wide range of peak shapes, so peak shapes are generated by a two-step process. The first step is to render curves that decay exponentially relative to the mean energy. These distributions may occur on either side or both sides of the mean depending on values of "low-E skew" and "high-E skew" parameters. The low-energy sides of these distributions also exhibit minor components that fall off more gradually than the principal exponential tail.[1] The computed distribution is smoothed with a symmetric Gaussian function. The broadening algorithm applies a cubic spline interpolation when spectra are computed, so that the peak shapes only need to be computed once after changing resolution parameters. As illustrated in Figure 6, this method enables an accurate replication of peak shapes for a broad range of detectors using only five adjustable parameters. Note that the resolution parameter in GADRAS only specifies the resolution of the Gaussian broadening function that is applied after construction of the exponential tails. Therefore, the

[1] A completely flexible description would contain separate parameters for the energy range of the exponential tails as well as magnitude terms for each component. The features could also be energy dependent. In order to avoid this complexity, GADRAS asserts associations for these relationships based on observations of peak shapes for numerous detectors.

mean width of the distribution for the CZT spectrum shown in Figure 6 is broader than a simple Gaussian peak with 0.85% resolution.

a)

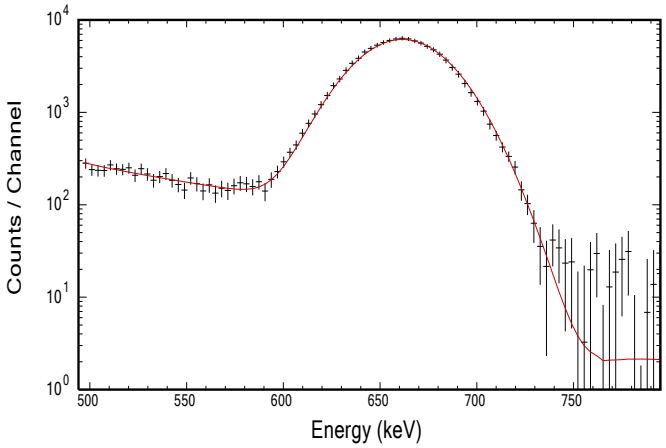

Detector Type:	NaI
Size:	2″×4″×16″
FWHM @ 661 keV:	8%
Low-E Skew:	0
High-E Skew:	0

b)

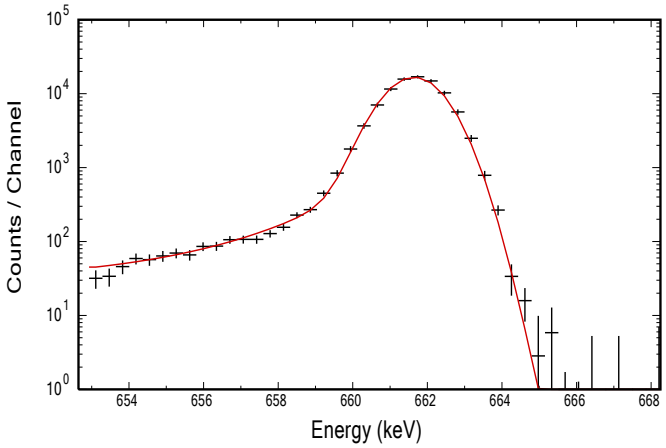

Detector Type:	HPGe
Size:	140%
FWHM @ 661 keV:	0.263%
Low-E Skew:	7
High-E Skew:	0

c)

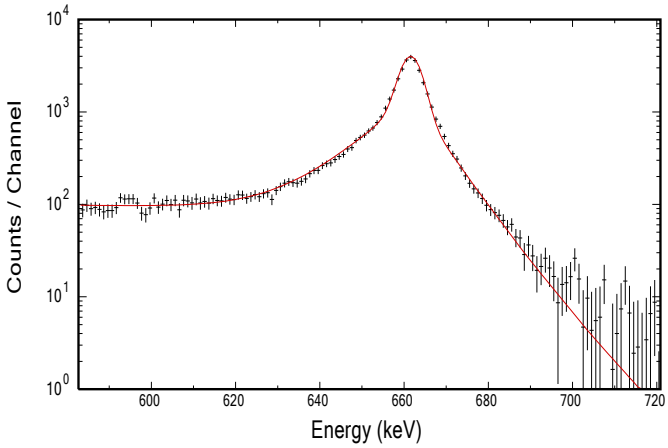

Detector Type:	CZT
Size:	18, 2 cm × 2cm × 1.5cm
FWHM @ 661 keV:	0.85%
Low-E Skew:	38
High-E Skew:	25

Figure 6. Computed spectra (red) are compared with measurements (black error bars) of ^{137}Cs sources that were recorded with NaI, HPGe, and CZT detectors. The types of detectors and the associated resolution parameters are shown to the right of graphs.

Doppler-broadened peaks are rendered by applying hard-coded underlying peak shapes for some of the more common Doppler-broadened emissions. The detector resolution function is applied to further broaden peaks, so that Doppler broadening may not be obvious in spectra that are recorded with low-resolution detectors. Figure 7 compares measured and computed spectra for an americium fluoride source, which exhibits numerous Doppler broadened peaks resulting from alpha-particles impinging on ^{19}F.

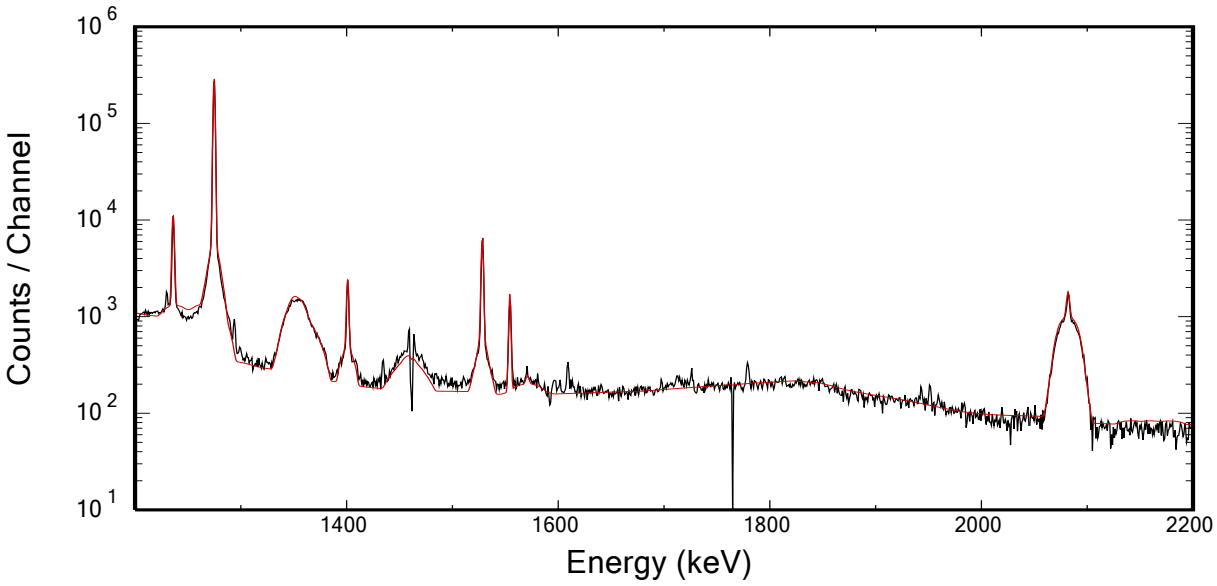

Figure 7. The computed spectrum (red) is compared with a measurement (black) of an americium fluoride source that was recorded by an HPGe detector.

3. RESPONSE FUNCTION PARAMETERS

Gamma-ray detector response function parameters are stored in a file named "Detector.dat" in the detector folder. These parameters are generally adjusted by editing the values that are presented on the *Detector* tab of the GADRAS Graphic User Interface (GUI). The parameters are clustered in frames according to the functionality. This section describes the significance of these parameters with respect to the response characteristics of gamma-ray detectors. Cyan backgrounds signify parameters that are selected for adjustment using the *Calibrate\Response Function* procedure. This procedure applies nonlinear regressions to adjust values of selected parameters to match one or more calibration measurements. Parameters are selected or de-selected by clicking on the parameter label. This section defines the use of parameters starting in the upper-left portion of the screen shown in Figure 8 and working to the lower right.

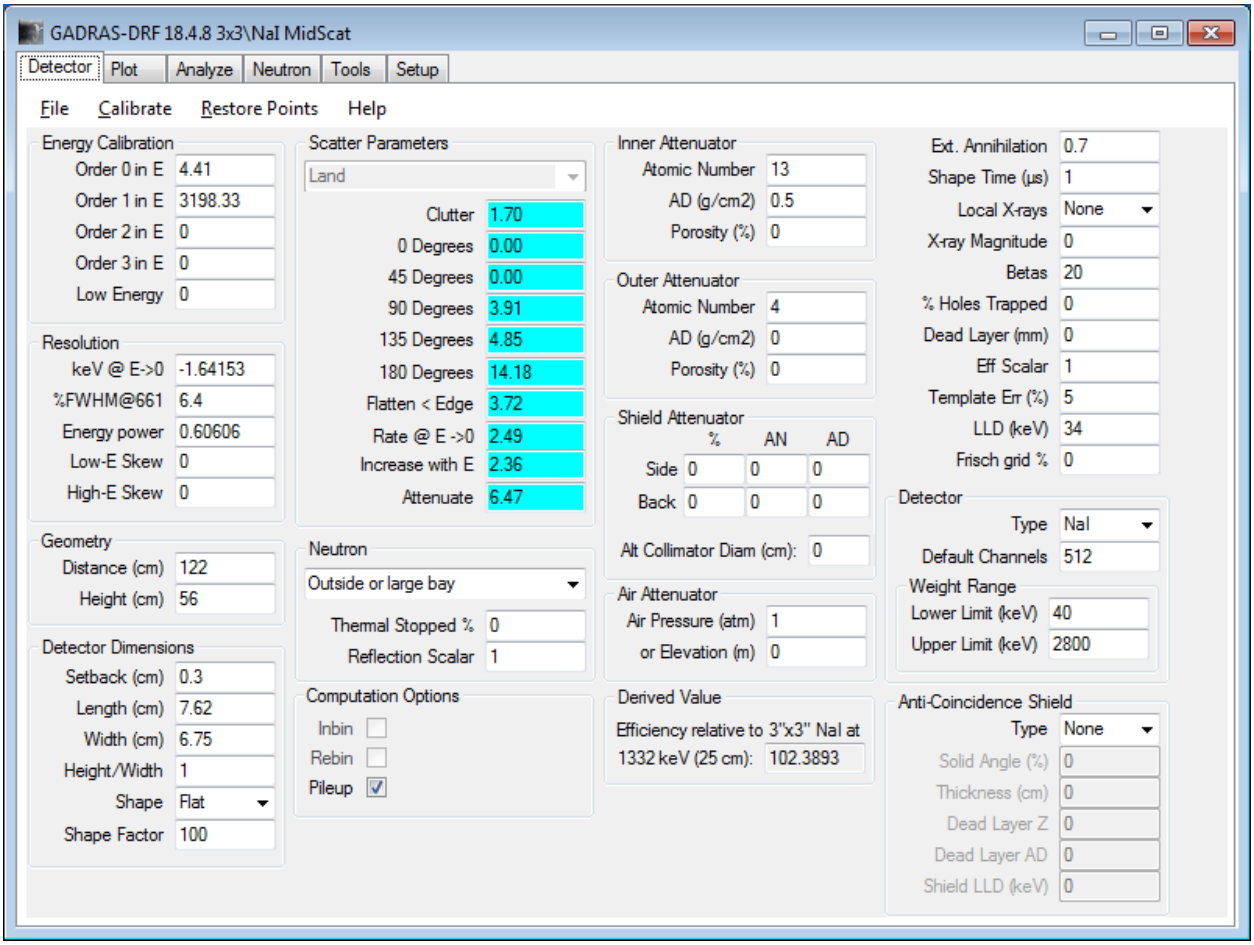

Figure 8. Screen capture showing response parameters for a 3″×3″ NaI detector.

3.1 Energy Calibration

3.1.1 Polynomial Coefficients

The most common energy calibration convention is to use polynomial coefficients. These coefficients convert channel number into energy at the lower edge of the channel according to the following equation:

$$E_i = c_0 + c_1 i + c_2 i^2 + c_3 i^3 + c_4 i^4 \quad (2)$$

where i is the channel number (starting at 0), and c_n is the n^{th} polynomial coefficient. GADRAS applies a convention defined as the *FullRangeFraction* in ANSI N42.42-2006, which represents energy calibration as follows:

$$E_i = a_0 + a_1 x + a_2 x^2 + a_3 x^3 + \frac{a_4}{(1 + 60x)} \quad (3)$$

where a_n is the n^{th} polynomial term which corresponds to c_n in Eq. (2), and x is the fractional energy of the spectral range. x ranges from 0 at the lower edge of the first channel and ends at 1 at the upper edge of the last channel. If the spectrum has uniform energy groups, $x=i/n$, where n is the total number of channels. The offset terms are identical in these definitions (i.e., $a_0=c_0$), and the higher order parameters are related as follows:

$$a_j = n^j c_j \quad (4)$$

The final term in Eq. (3), which addresses nonlinearity in the low-energy region, does not have an equivalent term in Eq. (2). However, neither a_4 nor c_4 is often applied, so this incompatibility is rarely important.

3.1.2 Deviation Pairs

Polynomial expressions are limited in their ability to replicate correlations between energy and channel number. Application of deviation pairs provides an alternative calibration method that can reproduce the energy array more precisely. Deviation pairs are generally applied by defining gain in offset terms according to Eq. (3), and using cubic splines to interpolate an array of energies and deviations. For example, gain and offset terms may be determined by the locations of the 239 keV and 2614 keV peaks associated with ^{232}Th. If the 1460 keV peak (from ^{40}K) is located in the channel corresponding to 1450 keV, a deviation of 10 keV should be declared at 1460 keV. The deviations are set to zero at mesh energies 239 keV and 2614 keV. GADRAS can process up to 20 deviation pairs. The deviation pairs are associated with specific spectra, so they are stored in GADRAS spectrum files, which have PCF extensions. ANSI N42.42-2011 files also accommodate deviation pairs, which are represented by the elements <EnergyValues> and <EnergyDeviationValues>. Deviations from linearity generally exhibit little temperature dependence; so energy calibration can generally be performed by only adjusting the gain parameter and retaining deviation pairs that were defined when detectors were characterized before deployment. In GADRAS, deviation pairs are accessed by clicking *Tools* followed by the <Deviation Pairs> button.

3.1.3 Energy Array

GADRAS is able to process spectra that specify non-linear energy bins. If spectra are provided in this way, the title of the first record in a multi-record spectrum file must be equal to the string "Energy". The energy array is applied exactly as specified if a_0 is equal to the lower edge of the first energy group and the full energy range is equal to a_1, with higher order terms in Eq. (3) equal to zero. Changing the energy calibration coefficients enables adjustment of the energy while preserving the general trend specified in the "Energy" record. This is accomplished by defining the parameter x in Eq. (3) according to the following relationship:

$$x = \frac{E_i - E_0}{E_{n+1} - E_0} \tag{5}$$

Where E_0 corresponds to the lower edge of the first channel and E_{n+1} corresponds to the upper edge of the last channel. This methodology allows GADRAS to process spectra that are represented with non-uniform energy group structures.

3.2 Resolution

If detector energy resolution followed Poisson statistics exactly, the width of the peaks would increase as the square-root of energy. However, the resolution of scintillators is often dominated by effects associated with the intrinsic nonlinearities. For semiconductor detectors, the resolution at the zero-energy asymptote is limited by dark current. For energies greater than 661 keV, GADRAS represents the full width at half-maximum height (*FWHM*) associated with the Gaussian broadening function according to the following equation:

$$FWHM = 6.61 * P_7\left(\frac{E}{661}\right)^{P_8} \quad (E > 661) \tag{6}$$

where *FWHM* is given in keV, P_7 and P_8 are response function parameters, and E is the gamma-ray energy in keV. The resolution of semiconductor detectors approaches an asymptotic low-energy limit, which is represented by the parameter P_6. If the energy is less than or equal to 661 keV, the resolution is defined by the following:

$$FWHM = \sqrt{\left[P_6\left(\frac{661 - E}{661}\right)\right]^2 + \left[6.61 * P_7\left(\frac{E}{661}\right)^{P_8}\right]^2} \quad (E \le 661;\ P_6 \ge 0) \tag{7}$$

where P_6 is given in units of keV. Eqs. (6) and (7) are equivalent if P_6 is zero. Eq. (7) does not accurately describe the resolution of scintillators, which generally exhibit better resolution at low energy than would be computed according to Eq. (5). In this case, P_6 will be less than zero. If the energy is less than 661 keV and P_6 is less than zero, the resolution is defined according to Eq. (8):

$$FWHM = 6.61 * P_7\left(\frac{\max(20,E)}{661}\right)^{P_8}^{\left[\frac{1}{\log(1 - P_6)}\right]} \quad (E \le 661;\ P_6 < 0) \tag{8}$$

Eq. (8) is an empirical relationship that reproduces the behavior of numerous scintillation detectors using the fewest number of adjustable parameters. The resolution at 661 keV is the same according to Eqs. (6) through (8), so transitions vary smoothly with energy.

GADRAS applies Eqs. (6) through (8) to compute the resolution for all types of detectors, but parameters that are displayed on the detector response function parameter page (see Figure 8) display values according to common conventions. Accordingly, the resolution parameter is represented in units of keV at 1332 keV for HPGe detectors; the resolution is specified as a percent of FWHM at 661 keV for other types of detectors.

3.3 Geometry and Detector Dimensions

The solid angle that is subtended by a detector is defined by the detector dimensions and the distance to a source [9]. All of the associated dimensions are specified in units of centimeters. The actual distance between the source and the detector crystal is equal to the sum of the distance parameter (P_{17}) and the setback parameter (P_{40}). The setback parameter is provided for convenience so that distances can be measured to the outside face of a detector enclosure rather than to the actual face of the detector material. Rather than specifying the height and width independently, the width and the height/width ratio are specified to avoid singularities if these parameters are adjusted simultaneously when detectors are characterized. The detector width is specified assuming detectors always have rectangular cross sections. The width must be scaled to preserve the cross sectional area for other shapes. If a source is located on the axis of a cylindrical detector with a diameter D, the detector width is computed according to the following relationship:

$$W = D\sqrt{\pi/4} \tag{9}$$

The detector length specifies the maximum chord length with respect to the source location. If the side of a cylindrical detector is exposed to a radiation source, the length parameter corresponds to the diameter, whereas the length of the cylinder is used for sources placed along the detector axis. The following equation defines the path length l distribution as a function of the shape parameter S:

$$l = \left(1 - \frac{r}{R}\right)^{\left(\frac{1}{S}\right)} \tag{10}$$

where r is the distance from the axis and R is the detector radius. Figure 9 illustrates path length distributions given by Eq. (10) for detectors with a variety of shapes. The shape parameter is set to a large value (~100) to describe rectangular cross sections, where all chords have approximately the same length. A value of about 3 is applicable to detectors with circular cross sections (e.g., the side of a cylindrical detector). Intermediate values of S can be used to describe shapes that do not conform to simple geometries, such as HPGe detectors with cavities along the detector axis. The profiles vary smoothly as the value of S changes, which facilitates fitting by nonlinear regression. The path length distributions are described from the perspective of a distant source. GADRAS adjusts path length distributions automatically when sources are close to the detector based on the distance parameter and detector dimensions.

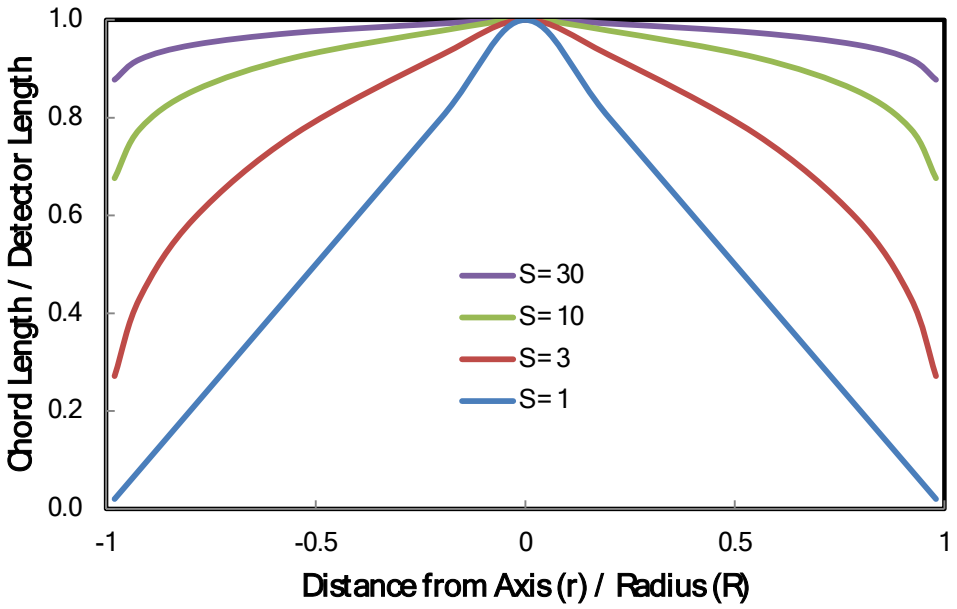

Figure 9. Path length distribution as a function of the shape parameter S.

3.4 Scatter Parameters

As described in Section 2.3, both first-principals and empirical descriptions of scattered radiation are applied to estimate the incidence of scattered radiation on detector surfaces. In order to retain general compatibility with older versions of GADRAS, the scatter parameters are scaled such that a nominal amount of environmental scatter is applied when the response function parameters are equal to 3. The clutter term varies as the inverse of the average distance to walls, and it is normalized such that the value equals 3 when the mean distance to the walls equals 3 meters. Parameters labeled "0 Degrees" through "180 Degrees" correspond to scalar terms. The parameters are applied by adjusting the intensity of scattered radiation using the Klein-Nishina formula. The magnitude of the estimated scatter flux is reduced proportionately with the value of the parameter if the value is less than 3. An empirical relationship is used to add scattering when the values of these parameters exceeds 3. Scattering within detector enclosures or scattering from additional objects in the vicinity of detectors are common factors that influence these parameters. Since these factors add to the total flux of scattered radiation on the detector surfaces, the scatter parameters generally exceed the nominal value of 3 for typical detectors.

The other scatter parameters are assigned somewhat descriptive names that represent effects associated with these parameters. For example, increasing the value of the parameter labeled "Attenuate" reduces the incidence of low-energy gamma-rays. These parameters apply empirical adjustments to the computed spectrum associated with gamma-rays that scatter before striking the detector. Detailed understanding of how these parameters affect computed spectra is not essential since the parameters are normally adjusted by nonlinear regression to match characterization measurements.

3.5 Neutron

Gamma-ray detectors generally exhibit a response when they are exposed to neutrons. GADRAS computes this response based on the neutron flux specified by the source file and applicable cross sections. A dropdown list describes the environment, which alters the neutron reflection based on a series of MCNP calculations. The following environments are included in the dropdown list:

- No reflection,
- Outside or large bay,
- Indoors above suspended floor, and
- Indoors above concrete on ground.

The parameter labeled "Thermal Stopped %" specifies the percent of thermal neutrons stopped by neutron absorbing materials around the detector. This parameter might have a non-zero value if the detector is surrounded by materials such as ^{6}Li or cadmium, which absorb thermal neutrons. The parameter "Relative Room Return" is a scalar that is applied to adjust the estimated flux of reflected neutrons.

3.6 Computation Options

The frame labeled "Computation Options" contains three check boxes that affect calculations.

- The box labeled "Inbin" is enabled if the detector folder contains a file named "Inbin.dat". This file defines the relative widths of successive energy groups, which are applied when the box is checked.
- If the "Rebin" box is checked, spectra are re-binned when they are plotted into the energy group structure defined by the file "Rebin.dat" in the detector folder. A command button labeled "Rebin Tool" on the *Tools* form facilitates construction of "Rebin.dat" files.
- Random pileup calculations are performed when the "Pileup" box is checked. Note that true coincidence pileup calculations are always performed if the source emits coincident gamma-rays and it is close enough for a significant number of coincidence events to register.

3.7 Inner and Outer Attenuator

The frames labeled "Inner Attenuator" and "Outer Attenuator" display parameters that represent materials placed between the detector and radiation sources. The Inner Attenuator describes materials that are in immediate contact with the detector, such as aluminum or steel casings that are generally present. The Outer Attenuator represents additional materials, such as tin filters that are used occasionally to reduce the intensity of low-energy gamma-rays. Each of these materials is characterized by a mean atomic number and areal density. Porosity parameters are generally set to zero, but positive values can be ascribed to represent voids in the outer attenuator. The attenuators are treated like any other material, and they add scattered radiation as well as reduce the intensity of radiation originating outside of the attenuating materials.

3.8 Shield Attenuator

The frame labeled “Shield Attenuator” describes materials imposed on the sides and back of the detectors. A common example would be a lead shield surrounding the circumference of a cylindrical detector. The atomic number would be 82 in this case and the areal density would be equal to the product of the thickness (cm) and the density (g/cc). The “Side %” parameter can also be used to describe collimators. Setting this parameter to 100 represents full coverage of the sides of the detector; setting the parameter to 200 declares that the shield extends in front of the detector to a distance that is equal to the length of the detector.

The parameter labeled “Alt Collimator Diam (cm)”, which defaults to zero, is provided to allow for collimators with diameters that are smaller than the diameter of the detector. If this parameter is greater than zero and the “Side %” parameter exceeds 100, the value of the “Alt Collimator Diam (cm)”, parameter is applied when the collimator aperture is computed. Otherwise, the detector diameter is used to compute the collimator aperture.

GADRAS imposes scattered radiation on all detector surfaces, and incorporates the specified shielding on the sides and back of the detector when necessary. Therefore, the shielding parameters alter the component of the spectrum derived from scattered radiation without necessitating adjustment of any of the scatter parameters.

3.9 Air Attenuator

Attenuation and scattering by air is computed if the air pressure exceeds zero. Air pressure can be specified by entering the atmospheric pressure or it can be estimated by entering the elevation.

3.10 Derived Value

The frame labeled “Derived Value” defines the detector photopeak efficiency at 1332 keV relative to a 3″×3″ NaI detector at a distance of 25 cm. This parameter, which is computed based on detector response parameters, is displayed for information purposes and it cannot be changed by user input.

3.11 Detector

The type of detector material is specified in the detector frame (lower-right corner of Figure 8). After creating a detector folder, changing this parameter only alters the interaction cross sections without adjusting the resolution parameters. This provides a convenient way to compare the performance of various detector materials without altering other parameters. The number of channels in the detector frame alters the default number of channels that are applied when spectra are computed without an associated measurement. The computed spectrum will use the number of channels in a measured spectrum if present. The weight range parameters designate the lower and upper limits (keV) that are used for computation of chi-square metrics and spectral fitting.

3.12 Anti-Coincidence Shield

The frame labeled “Anti-Coincidence Shield” characterizes effects associated with operating a detector in conjunction with anti-coincidence shields.

3.13 Miscellaneous Parameters

The upper-right corner of Figure 8 presents several response function parameters that are described below:

- "Ext. Annihilation" is a scalar that adjusts the intensity of 511 keV photons, which are created by positron annihilation following pair production reactions.
- The "Shape Time (μs)" parameter adjusts random pileup calculations. This parameter is approximately equal to the width of the preamplifier shaping time for detectors that do not contain pileup rejecters. The parameter should be set to the negative value of the shaping time to describe detectors with pileup rejecters.
- The "Local X-rays" field defines the element responsible for generation of X-rays as a result of interactions; this is normally associated with shield materials. The parameter "X-ray Magnitude" is a scalar that adjusts the intensity relative to those derived by application of X-ray production cross sections.
- The text box "Betas" is related to an archaic parameter that is no longer in use. This parameter was used to estimate the continuum produced by beta particles interacting with materials near the detector.
- The parameter labeled "% Holes Trapped" is used as an empirical term related to hole trapping by detectors such as CdTe. This parameter does not have quantitative significance.
- "Dead Layer (mm)" is used to compute effects associated with dead layers on the surfaces of detectors such as HPGe.
- "Eff. Scalar" is a scalar that adjusts the intensity of computed spectra. This parameter is equal to the total number of elements in sensors that sum the output of several elements. The parameters may be less than unity if part of the detector is covered by a shield that blocks most of the incident radiation.
- The "Template Err (%)" parameter defines the average percent error that is applied when the variance is estimated. Application of variance estimates is described elsewhere [10].
- The parameter "LLD (keV)" represents the lower-level discriminator setting.
- The parameter "Frisch grid (%)" represents the percent of events that are recorded between Frisch grid electrodes, which are used in conjunction with some CZT detectors. Events recorded in this region can produce up to twice the apparent full energy because both electrons and holes are counted; whereas holes are excluded for interactions within the bulk material.

REFERENCES

1. D.J. Mitchell, "*Sodium Iodide Detector Analysis Software (SIDAS)"*, Sandia National Laboratories Report SAND86-1473•UC-32 (1986).
2. D.J. Mitchell, Howard M. Sanger and Keith W. Marlow, "*Gamma-Ray Response Functions for Scintillation and Semiconductor Detectors, Nucl. Inst. and Meth. A276"* (1989).
3. D.J. Mitchell and J. Mattingly, *"Rapid Computation of Gamma-ray Spectra for One-Dimensional Source Models"*, American Nuclear Society 2008 Annual Meeting (June 2008).
4. D.J. Mitchell, L.T. Harding, J.K. Mattingly, and J.L. Barnett, *"Neutron Count Rate Calculation in GADRAS Version 15.3*, Sandia National Laboratory Report SAND2009-4321P (2009).
5. D.J. Mitchell, *"X-Ray Escape Calculations for Gamma-Ray Detectors"*, Sandia National Laboratories Report SAND2010-4958 (2010).
6. F. Biggs and R. Lighthill, *"Analytical Approximations for X-Ray Cross Sections III",* Sandia National Laboratories Report SAND87-0070-UC-34 (1988).
7. Glenn F. Knoll, "*Radiation Detection and Measurement"*, John Wiley and Sons, Canada (1979).
8. G.G. Thoreson, D.J. Mitchell, L.A. Theisen, and L.T. Harding, *"Environment Scattering in GADRAS"*, Sandia National Laboratories Report SAND2013-8673.
9. H. Gothe and H. Yagi, *"Solid Angle Subtended by a Rectangular Slit"*, Nuc. Inst. and Methods 96, pp. 485-486 (1971).
10. D.J. Mitchell, *"Variance Estimation for Analysis of Radiation Measurements"*, Sandia National Laboratories Report SAND2008-2302 (April 2008).

DISTRIBUTION

1	MS0155	C. Hall	6634 (electronic copy)
1	MS0782	D. Mitchell	6634 (electronic copy)
1	MS0782	L. Harding	6634 (electronic copy)
1	MS0899	Technical Library	9536 (electronic copy)


Sandia National Laboratories